PERIODICO di MINERALOGIA
established in 1930

Dipartimento di Scienze della Terra
Sapienza Università di Roma

An International Journal of
Mineralogy, Crystallography, Geochemistry,
Ore Deposits, Petrology, Volcanology
and applied topics on Environment, Archaeometry and Cultural Heritage

Extensional magmatism in a continental collision zone, Tafresh area, western central Iran: structural, geochemical and mineralogical considerations

Farkhondeh Khademi [1], Abbas Asiabanha [*,1], John Foden [2], Zeinab Davoodi [1]

[1] Deptartment of Geology, Faculty of Science, Imam Khomeini International University, Qazvin, Iran
[2] School of Earth and Environmental Sciences, Adelaide University, Adelaide, SA 5005, Australia

ARTICLE INFO

Submitted: October 2018
Accepted: December 2018
Available on line: December 2018

* Corresponding author:
asiabanha@sci.ikiu.ac.ir

DOI: 10.2451/2019PM822

How to cite this article:
Khademi F. et al. (2019)
Period. Mineral. 88, 1-18

ABSTRACT

The Tafresh area, located on the middle part of Urumieh-Dokhtar magmatic arc, is a suitable area for considering the effects of tectonic structures on development of the volcanic facies in the magmatic provinces. The main structure in the area is a dextral fault (so called Rahjerd Fault) that has produced the local extensional basins and also the parallel dyke swarms (or feeder dykes) on its both sides. So, the pyroclastic deposits, basaltic-andesitic lava flows, parallel dyke swarms were appeared by explosive subaqueous and then effusive subaerial eruptions and eventually a dioritic stock intruded in the volcanic pile. Petrologically, the magmatic rocks are belonged to the calcalkaline suite that had been changed and evolved in the magma chambers of local extensional basins in a collisional tectonic setting. The mineral chemistry and geochemical modeling as well as the coexistence of different mineral paragenesis of plagioclases (An_{47-72} and An_{17-37}), pyroxenes (diopside and pigeonite) and amphiboles (magnesiohastingsite and magnesiohornblende) reveal that the AFC process is a dominant process in the magma chamber. Also, according to geothermobarometric calculations, the investigated volcanic rocks of the area could be grouped into two types: one type with higher P-T (>6Kbar and about 900 °C) including Eocene pigeonite-magnesiohastingsite bearing andesites (PHA) and Miocene andesites and other with lower P-T (1-4 Kbar and 600-800 °C) including the Eocene diopside-magnesiohornblende bearing andesites (DHA) and the dioritic stock.

Keywords: parallel dykes; extensional basins; AFC; geothermobarometry; Tafresh; central Iran.

INTRODUCTION

Urumieh-Dokhtar magmatic arc (UDMA) located on the western Iran (Figure 1), was formed and evolved by collision of the Arabian and Iranian continental lithospheric plates following closures of Neotethys ocean during Alpine orogenies (e.g., Berberian and King, 1981; Alavi, 1994; Agard et al., 2005; Vincent et al., 2007; Horton et al., 2008; Morely et al., 2009). The NW-trending UDMA is the SW-border of central Iran microcontinetnt (Alavi, 1994) with a 1700 Km in length from Anatolian Fault in Turkey to Oman Line and 100-150 Km in width. It is characterized by two prominent lithologic and structural characteristics:

1) It contains a thick sequence (up to 3-4 Km) of volcaniclastic deposits, basic-acidic lava flows and subvolcanic intrusions with a calcalkaline affinity. Although the oldest magmatic event in UDMA is attributed to Jurassic (Jazi et al., 2012) or early Cretaceous (Alavi, 1994) and continued up to Quaternary (e.g., Agard et al., 2005; Omrani et al., 2008), most researchers (e.g.,

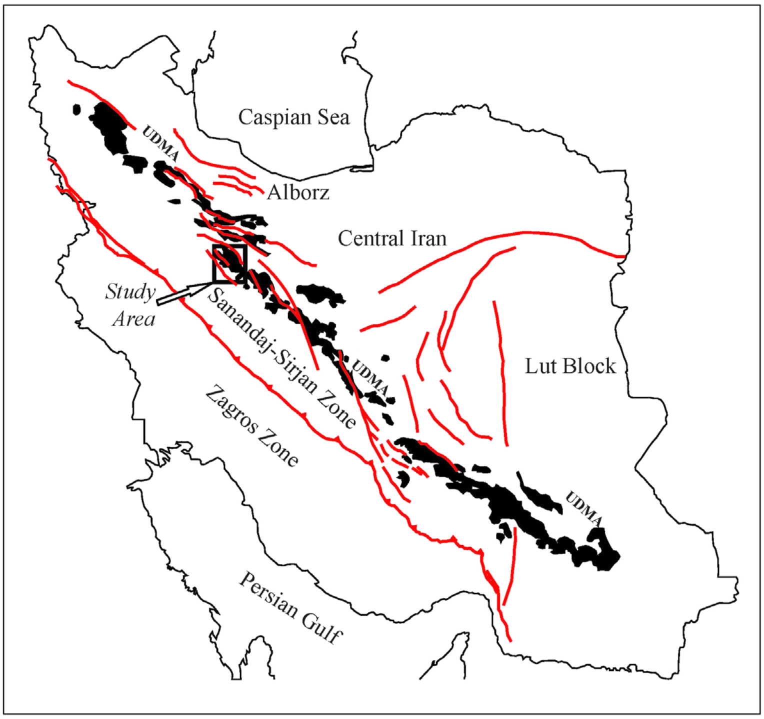

Figure 1. Situation of the study area (rectangle) in UDMA.

Stöcklin, 1974; Farhoudi, 1978; Omrani et al., 2008) suggest that the most widespread event in UDMA was occurred mostly in Eocene.

2) UDMA coincides to a NW-trending strike slip fault zone including North Tabriz Fault, Qom-Zefreh Fault and Dehshir-Baft Fault. It seems that this fault system played an important role in displacement of structures and likely volcanism in UDMA.

Thus, this study focuses mainly on the interplay between volcanism and tectonism in a magmatic arc via facies analysis, geochemical considerations and structural analysis.

LITHOSTRATIGRAPHY AND PETROGRAPHY

Urumieh-Dokhtar volcanic zone of Schröder (1944) is an Andean-type magmatic arc that has been active from late Jurassic to the present (e.g., Berberian and King, 1981; Berberian et al., 1982). However, Silurian volcanism has been reported in it recently (Tabatabaeimanesh et al., 2011).

The UDMA is mainly composed of voluminous calcalkaline and K-rich alkaline intrusive and extrusive rocks with associated pyroclastic and volcaniclastic successions (e.g., Jung et al. 1976; Ahmad and Posht Kuhi, 1993; Agard et al., 2005; Omrani et al., 2008; Dilek et al., 2010). The oldest rocks in the UDMA are calcalkaline intrusive bodies, which cut across late Jurassic formations and are overlain unconformably by lower Cretaceous fossiliferous limestones. On the other hand, the youngest rocks in this zone are Plio-Quaternary lava flows and pyroclastic deposits (Berberian and Berberian, 1981).

Ballato et al. (2011) suggest a two-stage collision process for Arabia-Eurasia collision zone, involving the “soft” collision of stretched lithosphere at first and “hard” collision following the arrival of unstretched Arabian continental lithosphere in the subduction zone. During this evolution, the tectonic regime shows a changeover from extensional (in Eocene) to contractional (in Oligocene-Miocene) regime.

The main Cenozoic magmatic episodes in UDMA are as follows (Förster et al., 1972; Amidi et al., 1984):

1. Effusion of alkaline and intermediate lavas in upper Paleocene-lower Eocene.
2. Deposition of volcano-sedimentary successions by early-middle Eocene phreatomagmatic eruptions.
3. Eruptions of dacitic-rhyolitic pyroclastic rocks and or dacitic domes formed by subaerial eruptions after uplifting the volcano-sedimentary basin during Pyrenean orogeny.
4. Deposition of marine Qom Formation in Oligocene-Miocene times together with alkaline lava flows.
5. Subaerial andesitic eruptions and small intrusions in lower Miocene.
6. Explosive and effusive eruptions with acidic intermediate in composition in upper Miocene-Pliocene.

The magmatic sequence of the studied area can be discriminated into three main facies based on lithostratigraphy and age relations (Figure 2): 1) Eocene volcanics; 2) Sub-volcanic bodies; 3) Miocene lavas.

Eocene volcanics

Most volcanic edifices which cropped out in the study area contain the Eocene pyroclastic deposits and volcanic rocks underlain by Cretaceous limestones with an angular unconformity and overlain by Oligocene and Miocene Formations (Emami, 1991). This facies is in turn subdivided into three sub-facies:

Volcano-sedimentary deposits

The sedimentary-pyroclastic succession of the Tafresh area is initiated with the Paleocene conglomerate equivalent to Kerman Conglomerate (Huckriede et al., 1962) contained rounded clasts (up to 40 cm in size) and followed by Eocene sedimentary (tuffaceous sandstone, shale, marl and limestone) and green pyroclastic (lithic-crystal tuff and crystal tuff) rocks (Figure 3a). The latter deposits contain benetic microfaunas (such as *Operculina, Ditrup* (Figure 3b)*, Discocyclina, Numulites*) and graded bedding. Because of this, it may be inferred that the shallow-depth sedimentary basin had been interrupted by subaqueous explosive eruptions.

Andesitic lava flows

The folded volcano-sedimentary deposits are overlain by andesite (including pyroxene- and amphibole andesite) and basaltic andesite. Because of the occurrences of the redden soil horizons under lava flows (Figure 3c) and also columnar joints (Figure 3d), it can be stated that the effusive eruptions had been occurred in a subaerial setting after uplifting the basin due to a compression regime.

Petrographically, these lava flows are characterized by porphyritic, megaporphyritic, intersertal and glomeroporphyritic textures and major minerals of plagioclase (andesine-labradorite), diopside, augite, hypersthene, amphibole (magnesiohastingsite and magnesiohornblende) as well as minor minerals such as titanomagnetite and ilmenite. Plagioclase phenocrysts show oscillatory zoning and sieve textures and pyroxene phenocrysts show zoning and exsolution lamellae. Also, many amphibole phenocrysts show evidence of transformations after pyroxenes.

Thin ignimbrite sheet

There is a limited and thin (10-20 m in thick) outcrop of rhyolitic ignimbrite with an autaxitic texture and phenocrysts of plagioclase, sanidine, quartz and to a lesser extent, pyroxene and opaque minerals.

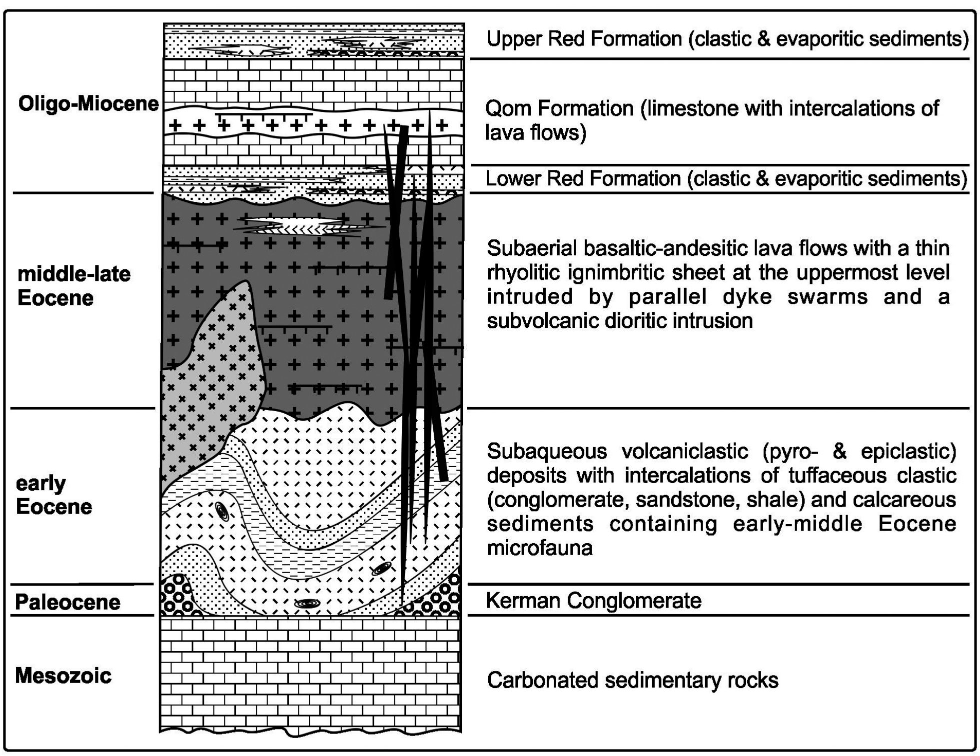

Figure 2. The facies-stratigraphy interactive column for volcano-sedimentary succession in the Tafresh area (without scale).

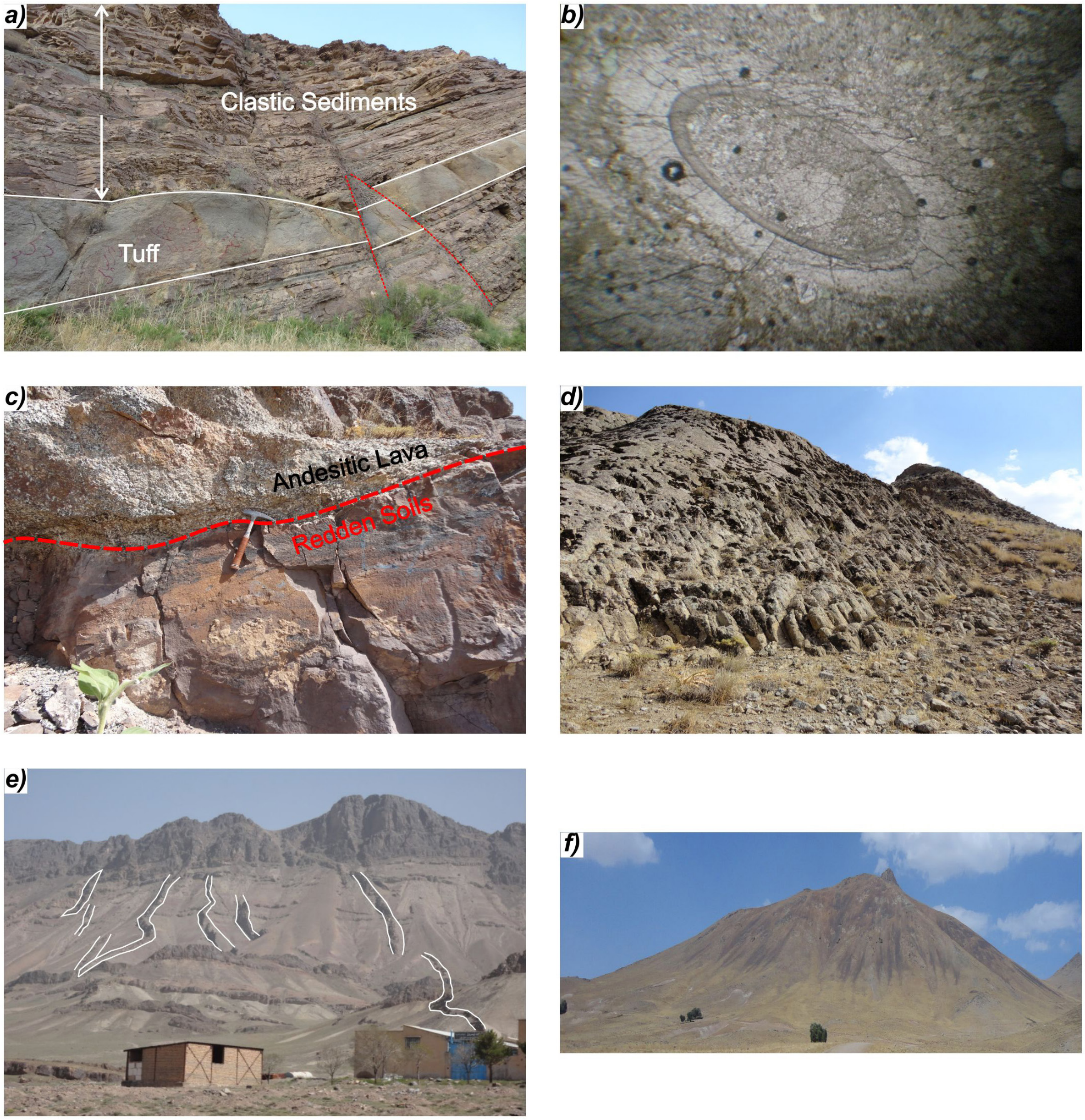

Figure 3. The selected figures from volcanic facies in the Tafresh area: a) intercalations of clastic and pyroclastic deposits; b) *Ditrup* microfossil characterizing Ypresian (early Eocene) in the calcareous sediments; c) the Eocene andesitic lava flow above the marl unit and formation of the redden soil at their contact; d) columnar joint in the the Eocene andesite lava flow; e) the parallel dyke swarms injected in the succession of lava and pyroclastic deposit succession (NE Tafresh); f) dioritic stock intruded in the Triassic sediments of Zaghar area.

Subvolcanic bodies

Parallel dyke swarms

The parallel dyke swarms are seen in eastern and western sides of Tafresh city (Figure 3e). They have 20-30 m in length and 2-5 m in width and their dominant striking is N40-45W and N10-20W. Because of their localization in the area with the greatest volume of lava flows, it may be regarded them as the feeder dykes through which the andesitic lava flow reached to the surface.

Dioritic intrusion

The only intrusive body in the area is a dioritic body that injected as a stock in the Triassic sediments (Figure 3f). The samples show zoned plagioclase and amphibole phenocrysts in a microgranular groundmass.

Miocene lavas

These andesitic lava flows have limited outcrops in UDMA (e.g., Bolourchi, 1979; Omrani et al., 2008).

In the study area, a 20-50m lava flow interlayer is seen in the Miocene Qom Formation (Figure 2). Petrographically, it is composed of zoned plagioclase, augite, amphibole (tschermakite and magnesiohastingsite) and titanomagnetite phenocrysts.

GEOCHEMISTRY

For geochemical whole-rock considerations, 9 fresh samples of various rock types were selected and analyzed by XRF and ICP-OES methods (Table 1). Samples were crushed and pulverized to 60-70μm. Whole-rock major elements were determined by XRF spectrometry (Philips MagiXPRO pw2540) after the preparation as the pressed pellets containing 4 grams of each sample and 0.8 gr Hoechst Wax-C after homogenizing in an agate mortar. The trace and rare earth elements were analyzed by ICP-OES method (Varian-735Es). 0.5 g of each sample was mixed by 10 ml hydrofluoric acid and 3 ml of perchloric acid and finally was heated up to 160 °C. The volume of solution should be about 1-2 ml which after cooling, 2 ml nitric acid and 3 ml of hydrochloric acid would be added to it to gain a clear solution for analysis.

For mineralogical surveying, 2 samples (28 points) in RomaTre University (Italy) and 6 samples (343 points) in University of Adelaide (Australia) were analysed by electron microprobe method. Mineral analyses were obtained with a CAMECA SX51 (15 KV, 20 nÅ) electron microprobe at the University of Adelaide, Australia and with a CAMECA SX50 (15 KV, 15 nÅ) electron microprobe at the RomaTre University, Italy.

Whole rock geochemistry

As shown in Table 1 and Figure 4, the samples are belonged to subalkaline suite with a calc-alkaline affinity (SiO_2=54.4-72.4; Na_2O+K_2O=2.8-7.7; Na_2O-2<K_2O). Based on the chondrite-normalized REE (Figure 5a) and primitive mantle-normalized multi-element spiderdiagrams (Figure 5b), they show many characteristics of subduction zone magmas including: LREEs enrichment relative to HREEs, negative anomaly of Nb and Ti and also strong positive anomaly of Pb. However, they don't show any negative anomaly of Ta, as a distinctive geochemical signature of subduction zone magmatism. Enrichment of LILEs and positive anomaly of Pb and U could be produced by fluids emanated from subducting lithosphere into the mantle wedge and addition of plagic sediments into the melting source, respectively (Rollinson, 1993; Tatsumi et al., 2002; Varekamp, 2010). Also, the subcontinental lithospheric mantle can be envisaged as another alternative source for these enrichments.

On the other hand, most samples occupy the field intercontinental rift of Cabanis and Lecolle (1989) diagram (Figure 6a) and within plate volcanic zone (WPVZ) field of Gorton and Schandl (2000) diagram (Figure 6b) and lie near the OIB magmatic source (Figure 6c). Kumar et al. (2015) suggest that La/Nb ratio is a useful geochemical proxy for distinguishing melts derived in subduction-zone and rift-zone settings. Accordingly, the studied samples set in the rift-related magmas (Figure 6d). Also, they set in the transitional region between the island arc and within-plate fields of Condie (1989) and D'Orazio et al. (2004) plots (Figures 6 e,f). Thus, we propose a subduction-related magma source in an intercontinental extensional regime.

Also, because of high amount of Th (7.49-16.69), high ratio of Ba/La (>15) and positive anomaly of Pb, it can be stated that a crustal component together with oceanic sediments had been played a considerable role in the chemical signatures of magma sources in the studied area (Wood, 1980; Fan et al., 2003).

Mineral chemistry

Feldspars

Based on the Figure 7, the composition of feldspars (Table 2) in the samples shows the following characteristics:

i) The phenocrysts and microliths in the Eocene lavas are labradorite (An_{47-72}) and Na-K feldspars (An_{17-37} and sanidine) in composition, respectively.

ii) The feldspars compositions in the dioritic intrusion show the same fields of Eocene lavas (An_{51-56} and An_{16-28}).

iii) An_{46-70} and K-feldspar (mostly anorthoclase) are the composition of feldspars in the Miocene lavas.

Pyroxenes

Whereas the pyroxene phenocrysts (Table 3) in the Miocene lavas are diopside in composition, the ones in the Eocene lavas set in two types (Figure 8a):

i) diopside (Fe#<0.2, low in Ti and high in Cr and Ca)

ii) pigeonite (Fe#>0.35, high in Ti and low in Cr and Ca).

Furthermore, many pyroxene phenocrysts of Eocene lavas show the exsolved lamellae and fall in the volcanic arc and within plate fields of Nisbet and Pearce (1977) and Leterrier et al. (1982) (Figure 8b).

Amphiboles

All amphiboles in the studied samples (Table 4) have mg# >0.5, Ca_B>0.5 (1.23-1.88) and Ti<0.5 (0.046-0.26). But, as shown in Figure 9, they are subdivided into two types:

i) magnesiohornblende (mg#=0.76-1, $(Na+K)_B$=0.27-0.48) in the diopside-bearing Eocene lavas and dioritic intrusion.

ii) magnesiohastingsite (mg#=0.73-1, $(Na+K)_B$=0.4-

Table 1. Major element (wt%) and trace element (ppm) data for volcanic rocks from the Tafresh area, central Iran.

Sample No.	14/F	4/E-1	11/A	9/E-2	11/F	10/F-6	1/F	6/E	C-1
	Eocene Lavas		Dyke Swarms		Dioritic Intrusion		Ignimbrite Sheet		Miocene Lavas
SiO_2	54.40	51.40	66.30	62.80	56.90	60.80	72.40	70.30	64.80
TiO_2	0.70	1.20	0.90	1.00	0.70	0.50	0.40	0.60	0.60
Al_2O_3	17.40	18.50	14.10	15.10	18.30	17.50	14.30	15.10	15.40
Fe_2O_3	9.80	9.50	6.90	7.80	7.10	6.30	1.50	3.30	5.40
MnO	0.20	0.10	0.10	0.10	0.10	0.20			0.10
MgO	4.20	2.70	2.40	2.80	3.00	2.80	0.30	0.80	1.50
CaO	8.20	7.30	0.80	1.50	6.80	5.20	1.30	0.80	5.90
Na_2O	2.20	2.70	3.90	4.00	2.60	2.70	1.90	2.80	2.40
K_2O	0.60	1.50	1.10	1.30	0.80	1.20	5.80	4.00	1.20
P_2O_5	0.10	0.20	0.20	0.40	0.20	0.20		0.10	0.30
LOI	1.89	4.66	3.08	3.00	3.24	2.60	1.93	2.05	1.95
Total	99.79	99.76	99.78	99.80	99.74	100.00	99.83	99.85	99.85
Cs	5.72	11.21	8.35	8.48	9.15	5.20	1.22	3.08	4.81
Rb	81.07	48.52	13.78	22.66	78.11	106	11.67	22.46	136
Ba	175	256	220	153	409	507	516	702	510
Sr	332	198	56	88	312	432	47	89	517
Pb	24.63	32.68	26.11	21.08	13.48	21.70	8.53	8.01	20.63
Th	15.73	15.95	12.53	12.25	14.14	9.56	12.97	7.49	16.69
U	4.60	8.96	6.17	6.28	7.42	4.24	0.54	2.40	3.96
Zr	238	344	286	332	247	122	68	392	331
Hf		8.65	1.73	6.27	9.25	6.98	8.55	10.46	13.38
Ta	4.99	7.96	3.20	2.00	2.28	2.25	0.88	0.99	1.99
Y	20.43	32.23	24.62	24.54	21.59	22.84	23.84	25.35	19.34
Nb	25.18	43.42	29.37	34.24	28.40	23.40	12.16	19.91	23.78
Sc	28.63	25.23	17.51	15.54	12.81	13.30	6.35	8.20	12.50
V	218	234	52	70	155	106	19	27	131
Cr	101.72	16.12	19.78	16.74	18.53	28.36	19.64	73.12	17.67
Co	20.33	28.91	16.78	19.35	22.88	13.86	1.15	6.11	10.09
Ni	36.97	11.39		7.64	4.40	1.96	2.17	11.90	
Cu	32.32	44.60	9.37	5.42	22.33	18.86	9.42	3.92	30.94
Zn	69.35	152.51	168.16	222.85	140.94	78.77	16.76	50.65	52.57
Ga	18.27	20.24	17.97	19.41	24.80	13.87	8.84	15.40	14.29
Ge	1.19	3.01	2.17	2.09	2.31	1.22	< 0.4	1.02	1.37
As	4.53	17.59	0.50	4.00	6.04	2.62	3.30	12.88	9.82
Se		0.65	0.57			0.30			0.61
Ag		0.10	0.16	0.10	0.20			0.10	0.16
Cd						0.41	0.89		0.58
In	0.93	0.55			0.67	0.83			
Sn	4.49	4.07	3.12	3.46	3.75	3.14	0.82	1.44	3.44
W	1.09	1.83	1.30	1.67	1.59	0.91	0.77	1.01	1.12
La	8.50	16.06	11.65	10.96	14.46	20.71	30.85	19.67	20.85

Table 1. Continued ...

Sample No.	14/F	4/E-1	11/A	9/E-2	11/F	10/F-6	1/F	6/E	C-1
	Eocene Lavas		Dyke Swarms		Dioritic Intrusion		Ignimbrite Sheet		Miocene Lavas
Ce	22.43	41.75	21.93	22.16	34.66	42.46	64.29	37.49	41.36
Pr	6.68	7.40	8.49	6.76	6.07	9.26	14.73	6.31	10.00
Nd	11.01	21.54	7.31	7.48	11.76	21.19	32.07	19.01	13.35
Sm	1.73	4.20	2.32	2.64	5.07	4.25	6.09	3.69	4.38
Eu	1.07	1.89	0.80	0.92	1.14	1.17	0.44	1.09	1.28
Gd	5.82	6.43	4.59	5.22	5.36	5.12	2.78	3.95	4.94
Tb	1.07	0.98	0.78	0.81	0.85	0.76	0.24	0.43	0.74
Dy		8.57	5.72	4.14	1.53	1.33	9.55	8.98	2.56
Ho	0.99	0.91	0.58	0.61	1.03	0.90	0.49	0.42	0.93
Er	2.57	3.21	2.11	2.62	2.51	2.24	1.71	2.04	1.14
Tm	0.51	0.49	0.33	0.37	0.42	0.32		0.15	0.35
Yb	2.74	3.71	2.84	3.05	2.60	2.32	2.19	2.64	2.38
Lu	0.56	0.51	0.34	0.43	0.46	0.38		0.17	0.39

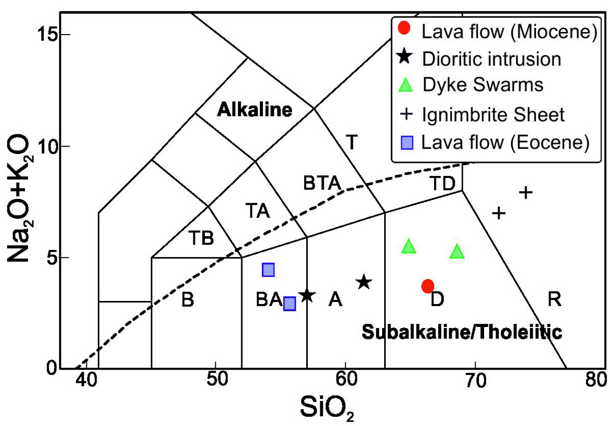

Figure 4. TAS classification diagram of Le Maitre et al. (2002). Abbreviations: A: andesite; B: basalt; BA: basaltic andesite; BTA: basaltic trachyandesite; D: dacite; R: rhyolite; T: trachyte; TA: trachyandesite; TB: trachybasalt; TD: trachydacite.

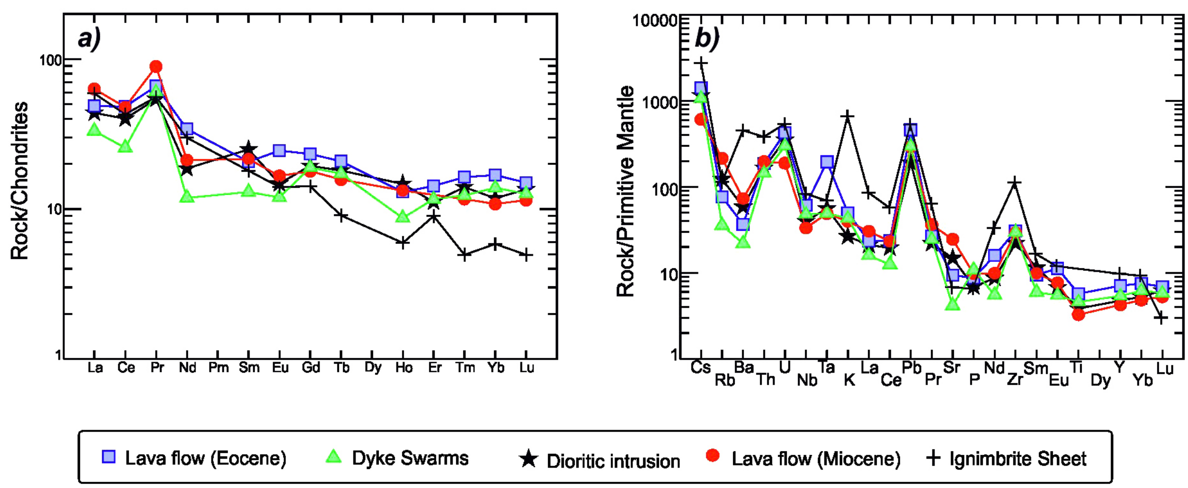

Figure 5. a) REE-spiderdiagram normalized by chondrite (Nakamura, 1974); b) multi-element spiderdiagram normalized by primitive mantle (Sun and McDonough, 1989).

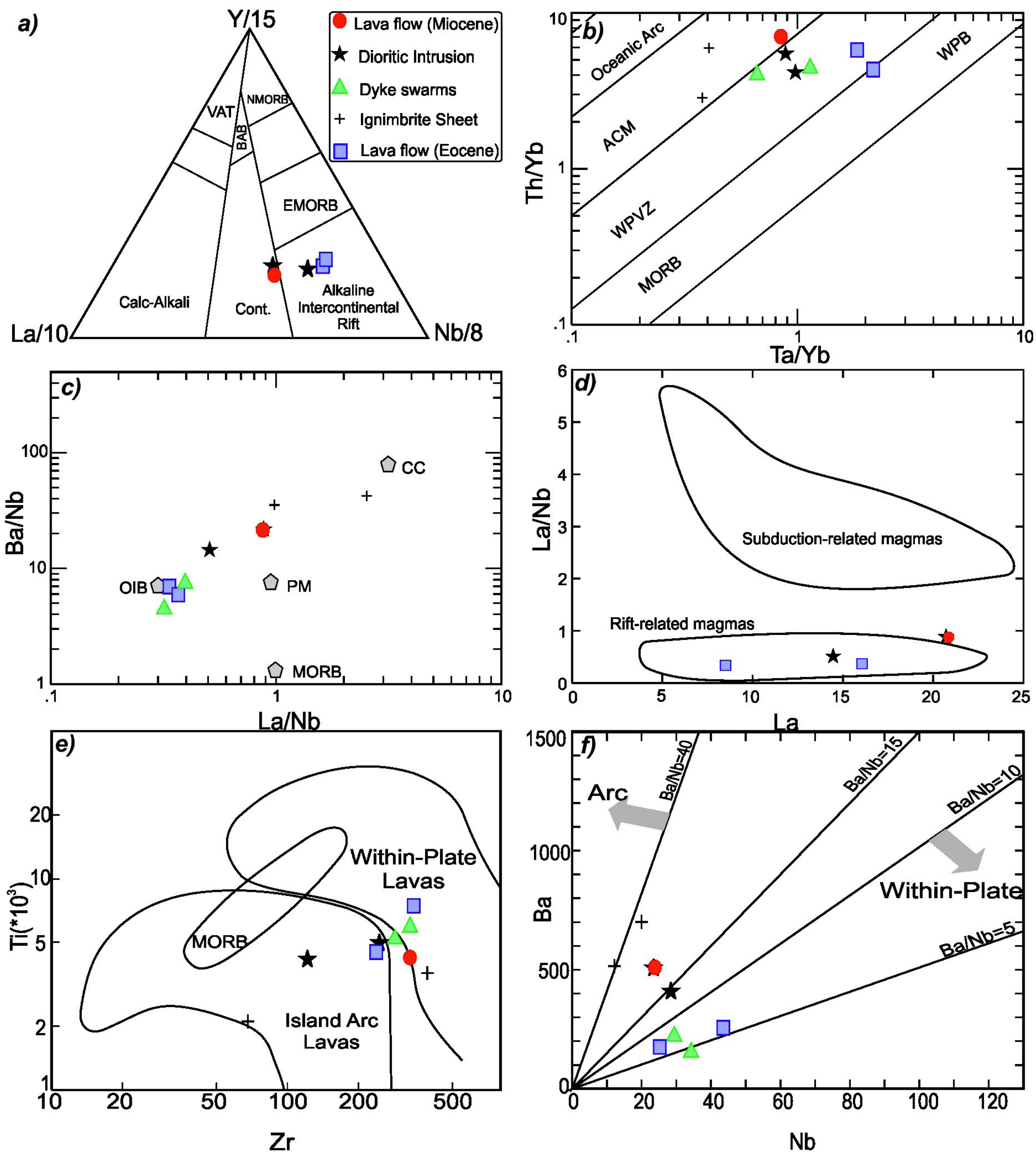

Figure 6. Tectonic discrimination plots: a) La/10-Y/15-Nb/8 plot (Cabanis and Lecolle, 1989); b) Th/Yb vs Ta/Yb diagram (Pearce, 1983 with changes from Gorton and Schandl, 2000) (ACM =Active Continental Margins; WPB =Within Plate Basalts; WPVZ =Within Plate Volcanic Zones); c) Ba/Nb vs. La/Nb plot (PM = primary mantle; OIB = ocean island basalt; MORB =mid-ocean ridge basalt; CC =continental crust) (data of PM, OIB, and MORB are from Sun and McDonough (1989), whereas CC data are from Rudnick and Gao (2003)); d) La/Nb vs. La plot (Kumar et al., 2015); e) Ti/Zr diagram of Condie (1989); f) Ba/Nb diagram of D’Orazio et al. (2004).

0.73, $^{VI}Al<Fe^{+3}$) in the pigeonite-bearing Eocene lavas and Miocene lavas.

So, we can discriminate the Eocene lavas into two mineralogical types: 1) diopside-magnesiohornblende-bearing andesites (DHA) and 2) pigeonite-magnesiohastingsite-bearing andesites (PHA).

Oxygen fugacity

According to Spear (1981) and Anderson and Smith (1995), oxygen fugacity of magmas can be calculated from Fe# vs Al^{IV} in amphiboles. Accordingly, as shown in Figure 10, all samples fall in the high oxygen fugacity field. As seen in Figure 10, the PHA show the higher

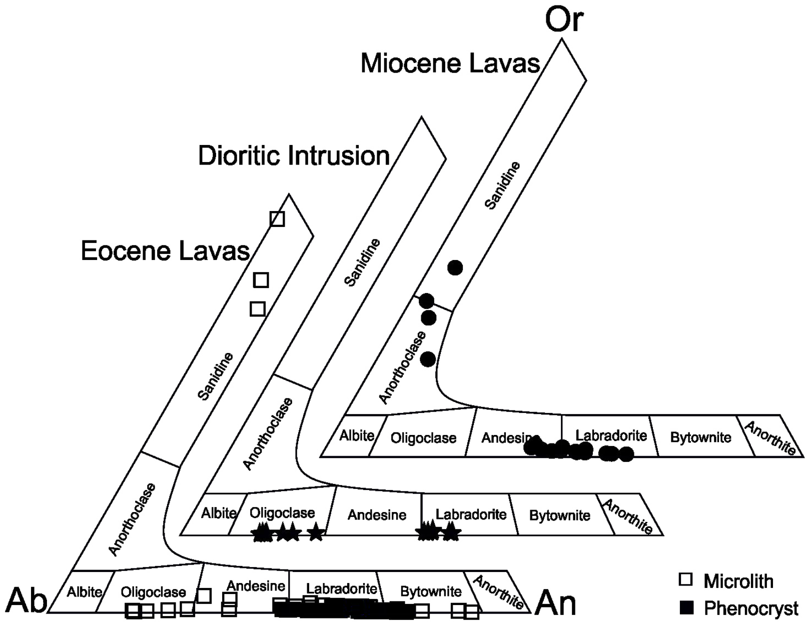

Figure 7. Chemical compositions of feldspars in the volcanic rocks of the study area plotted in an Or-Ab-An ternary diagram.

Table 2. Representative chemical compositions and calculated mineral formulae and modal mineral composition of feldspar.

	Eocene lavas						Dioritic intrusion				Miocene lava			
	Pl		Kfs				Pl		Kfs		Pl		Kfs	
Sample	14/F-1	14/F-1	14/F-1	14/F-1	14/F-1	14/F-1	10/F-6	10/F-6	10/F-6	10/F-6	C-1	C-1	C-1	C-1
SiO_2	54.59	49.46	64.17	65.47	65.08	68.22	54.88	53.32	64.27	65.53	55.89	52.09	66.34	67.91
Al_2O_3	26.64	31.46	20.38	19.39	23.57	23.85	27.38	28.13	22.60	23.00	27.12	29.48	20.91	19.64
Cr_2O_3	0.01	0.03	0.03	0.00	0.01	0.03	0.01	-0.02	-0.02	0.00	-0.02	0.00	-0.02	0.01
FeO	0.23	0.29	0.05	0.09	0.05	0.07	0.23	0.26	0.05	0.03	0.59	0.51	0.62	0.63
CaO	10.05	15.13	0.80	0.08	3.50	3.66	10.62	11.41	3.60	3.30	10.05	12.80	2.15	0.81
Na_2O	5.78	2.91	1.61	0.52	9.21	3.38	5.59	4.91	9.80	6.81	5.64	4.19	7.48	4.21
K_2O	0.14	0.05	12.09	13.80	0.11	0.07	0.13	0.11	0.09	0.07	0.39	0.10	3.96	5.73
Total	98.90	99.33	100.32	99.87	101.49	99.30	98.90	98.22	100.37	98.72	99.76	99.24	102.02	99.20
No. Oxygens	8	8	8	8	8	8	8	8	8	8	8	8	8	8
Si	2.52	2.28	2.93	3.00	2.82	2.93	2.50	2.46	2.83	2.88	2.53	2.39	2.91	3.02
Al	1.45	1.71	1.10	1.05	1.20	1.21	1.47	1.53	1.17	1.19	1.45	1.59	1.08	1.03
Fe^{2+}	0.01	0.01	0.00	0.00	0.00	0.00	0.01	0.01	0.00	0.00	0.02	0.02	0.02	0.02
Ca	0.50	0.75	0.04	0.00	0.16	0.17	0.52	0.56	0.17	0.16	0.49	0.63	0.10	0.04
Na	0.52	0.26	0.14	0.05	0.77	0.28	0.49	0.44	0.84	0.58	0.49	0.37	0.64	0.36
K	0.01	0.00	0.70	0.81	0.01	0.00	0.01	0.01	0.01	0.00	0.02	0.01	0.22	0.33
Total	5.01	5.00	4.92	4.90	4.97	4.60	5.01	5.00	5.01	4.81	5.00	5.01	4.97	4.80
%Or	0.80	0.27	79.52	94.11	0.63	0.87	0.76	0.62	0.51	0.54	2.26	0.60	23.09	44.72
%Ab	50.56	25.74	16.08	5.44	82.11	62.02	48.42	43.52	82.69	78.48	49.24	37.00	66.36	49.95
%An	48.63	73.98	4.40	0.45	17.27	37.11	50.82	55.86	16.80	20.98	48.50	62.40	10.55	5.33

Table 3. Representative chemical compositions and calculated mineral formulae and modal mineral composition of clinopyroxene.

	Eocene lavas										Miocene lava		
Sample	Cpx						Opx				Cpx		
	14/F-1	14/F-1	14/F-1	14/F-1	14/F-1	14/F-1	14/F-1	14/F-1	14/F-1	14/F-1	c-1	c-1	c-1
SiO_2	53.41	51.74	51.07	51.27	50.69	51.12	51.43	51.40	51.67	51.72	51.74	51.01	49.06
TiO_2	0.20	0.30	0.58	0.61	0.67	0.37	0.36	0.27	0.37	0.41	0.28	0.40	0.19
Al_2O_3	1.92	2.35	1.47	1.49	1.35	3.22	1.92	0.99	0.93	1.26	2.02	2.66	0.98
Cr_2O_3	0.12	0.19	0.00	0.02	-0.03	0.22	0.05	0.00	0.02	-0.02	0.00	0.00	0.00
FeO	5.33	7.05	14.64	14.37	16.94	8.12	20.03	19.03	20.23	19.16	9.33	8.47	9.34
MnO	0.18	0.18	0.39	0.37	0.48	0.29	0.52	0.63	0.57	0.63	0.47	0.27	1.13
MgO	17.99	16.63	14.38	14.33	12.24	16.59	18.19	18.29	18.62	16.97	15.36	15.05	15.08
CaO	20.77	19.88	15.69	16.04	16.18	18.42	6.05	7.34	5.67	8.64	20.12	21.71	20.93
Na_2O	0.24	0.21	0.24	0.25	0.27	0.27	0.44	0.12	0.09	0.16	0.25	0.28	0.46
K_2O	0.01	0.01	0.00	0.00	0.01	0.00	0.02	0.02	0.01	0.02	0.013	0.00	0.05
Total	100.17	98.54	98.47	98.73	98.80	98.73	99.08	98.11	98.11	98.95	99.58	99.84	97.23
No. Oxygens	6	6	6	6	6	6	6	6	6	6	6	6	6
Si	1.95	1.93	1.96	1.96	1.96	1.91	1.95	1.97	1.98	1.97	1.93	1.89	1.88
Ti	0.01	0.01	0.02	0.02	0.02	0.01	0.01	0.01	0.01	0.01	0.01	0.01	0.01
Al	0.08	0.10	0.07	0.07	0.06	0.14	0.09	0.04	0.04	0.06	0.09	0.12	0.04
Fe^{2+}	0.16	0.22	0.47	0.46	0.55	0.25	0.64	0.61	0.65	0.61	0.28	0.25	0.28
Mn^{2+}	0.01	0.01	0.01	0.01	0.02	0.01	0.02	0.02	0.02	0.02	0.01	0.01	0.04
Mg	0.98	0.93	0.82	0.82	0.71	0.92	1.03	1.04	1.06	0.96	0.85	0.83	0.86
Ca	0.81	0.80	0.64	0.66	0.67	0.74	0.25	0.30	0.23	0.35	0.80	0.86	0.86
Na	0.02	0.02	0.02	0.02	0.02	0.02	0.03	0.01	0.01	0.01	0.02	0.02	0.03
Total	4.01	4.01	4.00	4.00	4.00	4.01	4.01	4.00	4.00	4.00	4.00	4.00	4.00
%Wo	41.56	40.96	33.29	33.98	34.85	38.50	12.86	15.41	11.97	18.30	41.40	44.31	43.06
%En	50.12	47.70	42.46	42.26	36.68	48.25	53.86	53.42	54.70	50.03	43.95	42.72	43.17
%Fs	8.32	11.34	24.25	23.76	28.48	13.25	33.27	31.17	33.33	31.67	14.65	12.97	13.77

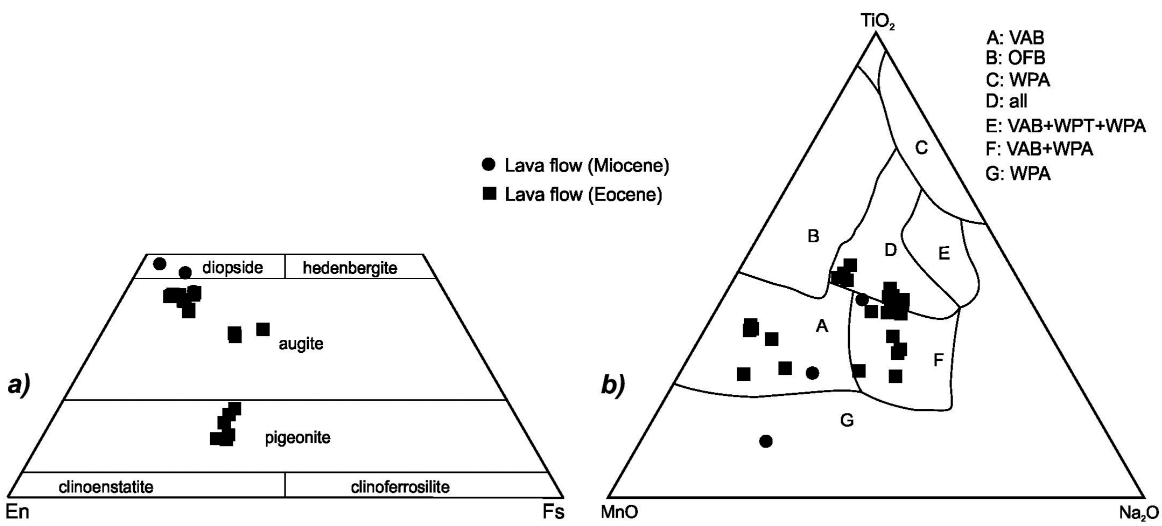

Figure 8. Chemical compositions of pyroxene phenocrysts plotted in: a) an En-Wo-Fs ternary diagram (Morimoto et al., 1988); b) a tectonic classification (Nisbet and Pearce, 1977).

Table 4. Representative chemical compositions and calculated mineral formulae of amphibole.

	Dioritic intrusion				Eocene lavas				Miocene lava			
	Am											
Sample	10/F-6	10/F-6	10/F-6	10/F-6	14/F-1	14/F-1	14/F-1	14/F-1	C	C	C	C
SiO_2	45.67	45.00	47.58	46.94	46.72	49.23	47.96	45.72	42.39	42.88	42.49	40.99
TiO_2	1.61	1.95	1.26	1.27	1.92	1.15	1.06	2.39	2.13	2.12	2.11	1.93
Al_2O_3	8.11	8.51	6.63	6.85	8.08	5.74	7.78	8.18	11.81	11.96	12.01	12.41
FeO	14.22	14.41	13.34	13.48	13.80	14.72	13.97	14.31	11.58	11.57	11.61	12.48
MgO	13.47	13.31	14.91	14.60	12.98	14.82	14.53	13.02	14.52	14.56	14.60	0.25
MnO	0.41	0.34	0.50	0.55	0.37	0.52	0.60	0.37	0.23	0.24	0.22	13.49
CaO	10.59	10.68	10.36	10.34	10.39	10.39	10.08	10.88	11.43	11.47	11.50	11.27
Na_2O	1.35	1.58	1.30	1.26	1.56	1.22	1.29	1.77	2.32	2.28	2.31	2.48
K_2O	0.20	0.23	0.15	0.15	0.22	0.15	0.12	0.25	0.40	0.39	0.38	0.44
Total	95.63	96.01	96.03	95.44	96.04	97.94	97.39	96.89	96.81	97.47	97.23	95.74
No. Oxygens	23	23	23	23	23	23	23	23	23	23	23	23
Si	6.86	6.75	7.05	7.02	6.88	7.10	6.93	6.72	6.19	6.21	6.17	6.60
Ti	0.18	0.22	0.14	0.14	0.21	0.12	0.11	0.26	0.23	0.23	0.23	0.23
Al	1.43	1.50	1.16	1.21	1.40	0.97	1.32	1.42	2.03	2.04	2.05	2.36
Al^{IV}	1.24	1.35	1.03	1.08	1.12	0.89	1.07	1.28	1.81	1.79	1.82	1.39
Al^{VI}	0.17	0.12	0.10	0.11	0.28	0.08	0.25	0.13	0.22	0.25	0.23	0.97
Fe^{2+}	1.78	1.81	1.65	1.68	1.72	1.80	1.71	1.78	23.00	23.00	23.00	23.00
Mn^{2+}	0.05	0.04	0.06	0.07	0.05	0.06	0.07	0.05	0.03	0.03	0.03	1.84
Mg	3.01	2.98	3.30	3.25	2.88	3.22	3.17	2.88	6.28	6.31	6.27	6.11
Ca	1.70	1.72	1.64	1.66	1.66	1.62	1.58	1.73	2.06	2.07	2.09	1.89
Na	0.39	0.46	0.37	0.36	0.45	0.35	0.37	0.51	0.50	0.48	0.50	0.51
K	0.04	0.04	0.03	0.03	0.04	0.03	0.02	0.05	1.43	1.42	1.43	0.70
Total Cations (S)	15.46	15.52	15.41	15.42	15.37	15.38	15.39	15.49	0.08	0.07	0.07	0.08

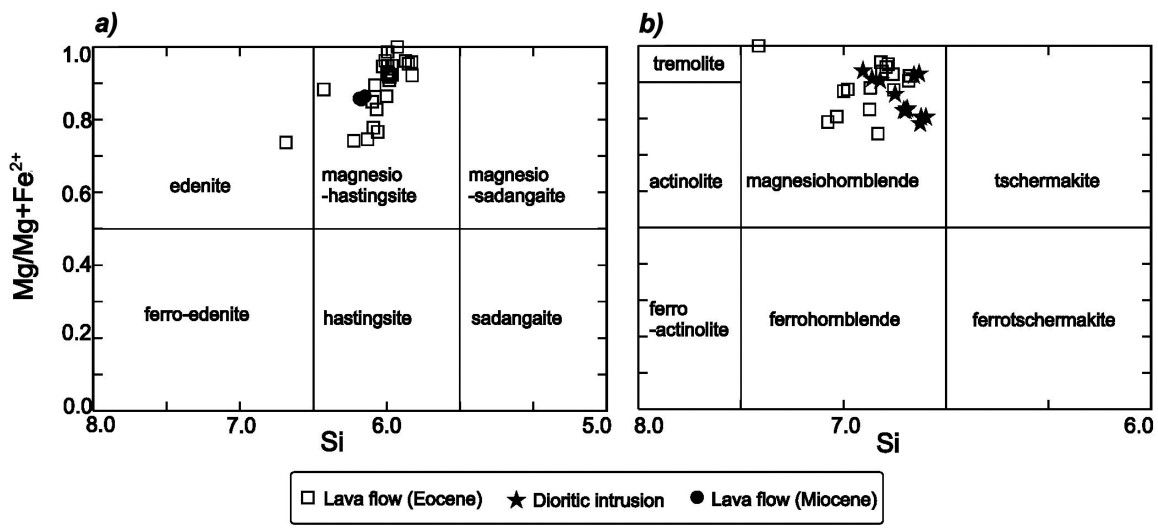

Figure 9. Chemical compositions of amphiboles (Leake et al., 1997): a) Eocene pigeonite-magnesiohastingsite bearing andesites (PHA) and Miocene lavas; b) Eocene diopside-magnesiohornblende bearing andesites (DHA) and dioritic stock.

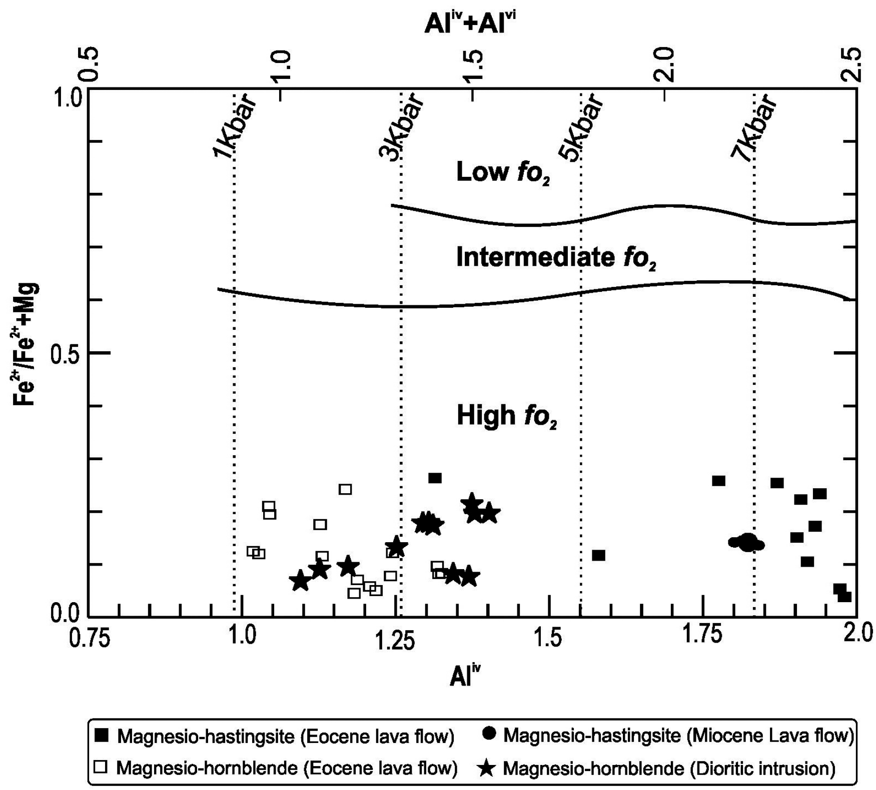

Figure 10. Fe# vs Al^{IV} plot for distinguishing of fugacities in amphiboles (Anderson and Smith, 1995) and Fe# vs Al^{IV}+Al^{VI} for defining of pressures in amphiboles (Smith, 1992).

Table 5. Results of geothermobarometric calculation for different volcanic facies of the Tafresh area.

Rock Unit		P (Kbar)		T (°C)	
Eocene Lavas	DHA*	1-4	Smidth (1992) Helz (1973)	620±20	Elkins and Grove (1990) Putirka (2008)
	PHA**	> 6		900±50	Lindsley (1983)
Dioritic Intrusion		2.5-4.5	Schmidt (1992)	685±10	Holland and Blundy (1994)
		2.5-4.2	Anderson and Smith (1995)	620±20	Elkins and Grove (1990) Putirka (2008)
		2.5-4.0	Ridolfi (2010)		
Miocene Lavas		6.5-8.5	Schmidt (1992)	720±10	Holland and Blundy (1994)
		5.8-8	Anderson and Smith (1995)	875±25	Ernst and Liu (1998)
		5-7	Ridolfi (2010)	1140±45	Elkins and Grove (1990) Putirka (2008)
		7.5	Ernst and Liu (1998)		

* Diopside-magnesiohornblende bearing andesite
** Pigeonite-magnesiohastingsite bearing andesite

pressure (>6 Kbar) than DHA (about 1-4 Kbar) in the Fe# vs ^{total}Al plot of Schmidt (1992).

Geothermobarometry

The results of geothermobarometric calculations on different magmatic facies by various methods (i.e., Al-contents in amphiboles (Schmidt, 1992; Anderson and Smith, 1995; Ridolfi et al., 2010), two feldspar thermometer (Elkins and Grove, 1990; Putirka 2008), hornblende-plagioclase pair thermometry (Holland and Blundy 1994) and two-pyroxene thermometry (Lindsley, 1983) have been given in Table 5. As shown in Table 5, Miocene lavas had been formed in higher *P* and *T* than Eocene lavas and dioritic intrusion. Thus, it can be postulated that the Miocene lavas had likely been originated from more depths.

AFC modeling

AFC modeling was based on the calculations of De Paolo (1981) using the sample 9/E-2 as the parent magma and the continental crust from Taylor and McLennan (1985, 1995) as the contaminant. As seen in the Ce/Pb vs Ba/Nb plot (Figure 11), the samples have a good fitness with AFC curves with r=0.7, but different D-values. Thus, it seems that the magma chamber had been open repeatedly for new pulses of magma and crustal components. Such a conclusion is verified by different mineral paragenesis of feldspars, pyroxenes and amphiboles (Figures 7-9).

STRUCTURAL ANALYSIS

The main structural elements in the study area recognizable on the satellite and aerial images as well as on the outcrops (Figure 12) are dominantly: i) reverse (thrust) faults with NW-SE strike-slip component; ii) dextral strike-slip faults with NNW-SSE striking; iii) folding with NW-SE striking associated with strike-slip faults. It seems that the strike of the folds has bent bearing of the fault (Figure 12).

According to many researchers (e.g., Nogol-Sadat, 1985; Walker and Jackson, 2004; Alavi, 2007; Morley et al., 2009), the main faults in UDMA, including Qom-Zefreh fault, Bidhend fault Dehshir-Baft fault, are basement faults. Nogol-Sadat (1985) and Mohajjel and Ferguson (2000) propose that the dextral transpressional system in UDMA activated the basement faults. On the other hand, the releasing and restraining zone could be produced by en-echelon pattern of dextral strike-slip faults in UDMA (Babaahmadi et al., 2010). Moreover, there are some overlaps between the compressional terminations of the dextral faults in the area. So, whereas such a structural regime produced the NW-SE striking folds, the parallel dyke swarms have been concentrated on tension gash zone on both sides of Rahjerd fault (Figure 12).

Moreover, Nogol-Sadat (1978) propose the Tafresh, Indes, Talkhab and Chaghar faults as the main dextral faults (N125-130E) and Bidhend fault (N160-170E) as a minor extensional fault in UDMA that was likely had been involved in Cenozoic volcanism. So, because of parallel striking of both Rahjerd and Bidhend faults and also the concentration of parallel dyke swarms on both sides of the Rahjerd fault, it can be stated that the Cenozoic volcanism in the area had been occurred by the extensional role of Rahjerd fault. Also, it seems that the N10-20W dyke swarms were produced by reactivation of Rahjerd fault and its local extension. Accordingly, the latter dyke swarms must be younger than the N40-50W dyke systems.

DISCUSSION AND RESULTS

Urumieh Dokhtar magmatic arc (UDMA) on the western Iran is a volcano-plutonic zone that proposed by most researchers (e.g., Berberian and King, 1981; Alavi, 1994; Agard et al., 2005; Vincent et al., 2007; Horton et al., 2008; Morely et al., 2009) as a result of subduction of Neothetys oceanic lithosphere and then continental collision of Arabia and central Iran microcontinents. On the other hand, it proposes that the main strike-slip faults (Qom-Zefreh, Dehshir-Baft and Bidhend faults) in this zone played an important role in the magmatic episodes. Because of this, UDMA could be imagined as a fault zone for reaching the magma to the surface.

In the study area located on the middle part of UDMA

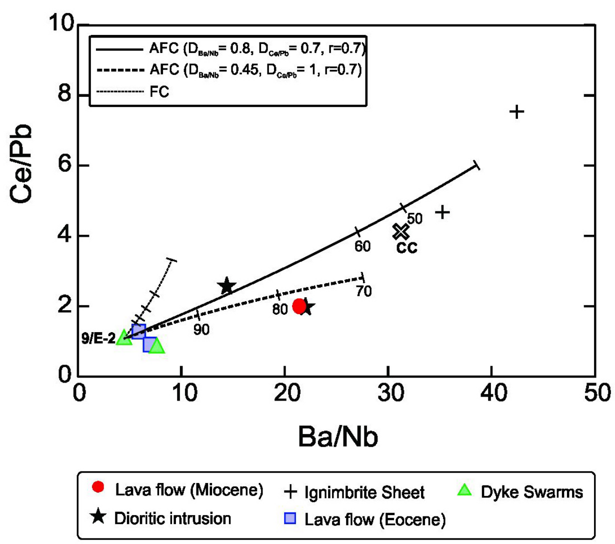

Figure 11. Geochemical modeling for studied samples on Ce/Pb vs Ba/Nb diagram. Note to better fitness of AFC trends than FC trend. The sample No. 9/E-2 have been selected as parental magma (C0) and continental crust (Taylor and McLennan, 1985, 1995) is contaminant (Ca).

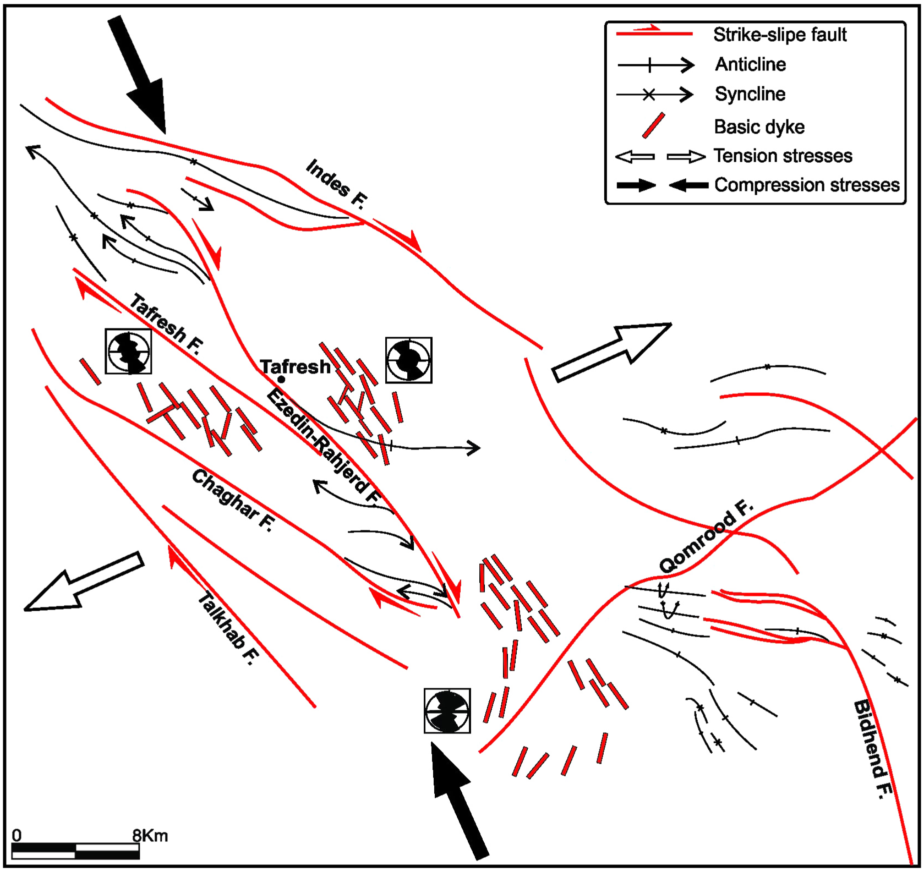

Figure 12. The structural map and the main stress vectors in the studied area. The major shortening trend is based on Hessami et al. (2003).

(near Tafresh city), there are different Cenozoic volcano-sedimentary and volcanic facies. The greatest thickness of lava flows are observed in the places with the parallel dyke swarms. Thus, we call them as feeder dykes. A structural analysis on dyke swarms and faults and folds in the area show that the dyke swarms have been localized on the both sides of the Rahjerd dextral fault (tensional gash zones) (Figure 12). As a result, we suggest that the volcanism in the Tafresh area is a “passive volcanism” during the strike-slip faulting.

Such a tensional regime is verified by lithological changes in the succession in which lower Eocene shallow-depth volcano-sedimentary deposits are followed by the calcalkaline lava flows. According to most researchers in last decades (e.g., Vincent et al., 2005; Ballato et al., 2011; Verdel et al., 2011; Rezaeian et al., 2012), the Eocene magmatism in UDMA was occurred in an extensional regime accompanied by crustal subsidence (Rezaeian et al., 2012). Also, Vincent et al. (2005) suggest that the magmatism and deposition have taken place in an extensional to transtensional setting, possibly caused by roll-back of the subducting Neotethys lithosphere (Vincent et al., 2005; Verdel et al., 2011). Although, the samples preserve some subduction-related characteristics (such as negative anomaly of Nb and to a lesser extent of Ti, strong positive anomaly of Pb and also enrichment of LILEs), they don’t show negative anomaly of Ta (as a distinctive signature of subduction mechanism). Moreover, they fall in the rift-related or within-plate fields of tectonic diagrams of Cabanis and Lecolle (1989) (Figure 6a), Gorton and Schandl (2000) (Figure 6b) and Kumar et al. (2015) (Figure 6d) and or in the transitional region between the island arc and within-plate of Condie (1989) and D’Orazio et al. (2004) plots (Figures 6 e,f). On the other hand, the pyroxene minerals set in both field of VAB and WPA in the diagram of Nisbet and Pearce (1977) (Figure 8b).

Heterogeneous characteristics of the volcanic samples are confirmed by mineral chemistry. It means that the Eocene andesites are subdivided into two subgroups: one having diopside and magnesio-hornblende (DHA) that show shallower pressure (<4Kbar) and other having pigeonite and magnesio-hastingsite (PHA) were originated at greater pressure (>6Kbar). Geothermobarometric calculations

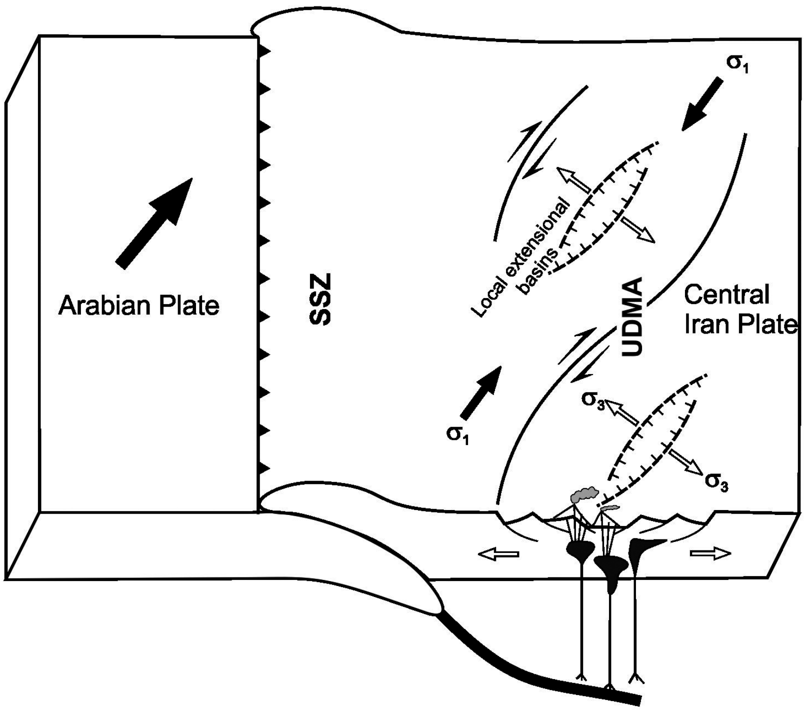

Figure 13. A Schematic model for producing the local tensional basins (tensional gash) between dextral faults in UDMA. Oblique movement trend of Arabian plate is based on Allen et al. (2004).

reveal that DHA and PHA have similar conditions with diorites and Miocene andesites, respectively. On the other hand, the AFC process could be concluded as the dominant process for explaining of magmatic evolution in the area. It can be imagined that the primary magma (with a subduction affinity) had been evolved in the crustal chambers by fractional crystallization and crustal contamination (Figure 13). The dextral fault system in the area (mainly Rahjerd fault) had produced the local extensional basins (Figure 12). The similar process has been reported for intra-arc basins in the Peruvian Andes by Polliand et al. (2005). According to Polliand et al. (2005), dextral wrenching was a trigger for the formation of a series of pull-apart basins and the emplacement of the Coastal Batholith in the Peruvian Andes.

The structural and petrological considerations of this study have given the following results:

1- The volcano-sedimentary succession in the Tafresh area occurred mainly during two consecutive stages: subaqueous and then subaerial stages that produced three major facies: Eocene volcanics (including volcano-sedimentary deposits, andesites and rhyolitic ignimbrites), subvolcanic bodies (including parallel dyke swarms and dioritic intrusions) and Miocene andesites.

2- Geochemically, the magma formed in a subduction- and collision-related setting, was evolved by crustal contamination processes in the extensional continental environment through the AFC process.

3- The mineral assemblages confirm the unstable conditions in the magma chamber. It means that the Eocene andesites have two different generation of plagioclases (An_{47-72} and An_{17-37}), pyroxenes (diopside and pigeonite) and amphiboles (magnesiohastingsite and magnesiohornblende). Because of this, we have subdivided them into two types: diopside and magnesio-hornblende andesites (DHA) and other pigeonite and magnesio-hastingsite andesites (PHA).

4- Geothermobarometric and mineral chemistry considerations reveal that the DHA and dioritic body have similar conditions (1-4 Kbar and 620-850 °C). Whereas, PHA and Miocene lavas show higher pressure and temperatures (>6 Kbar and about 900 °C).

5- The dextral strike-slip fault systems in the area produced the local extensional basin (or tensional gashes) for ascending the magma to the surface through feeder dykes.

6- As a result, we suggest the local extensional basins due to reactivation of NW-SE dextral strike-slip faults for appearance and evolution of different magmatic facies in the Tafresh area.

REFERENCES

Agard P., Omrani J., Jolivet L., Mouthereau F., 2005. Convergence history across Zagros (Iran): constraints from collisional and earlier deformation. International Journal of Earth Sciences 94, 401-419.

Ahmad T. and Posht Kuhi M., 1993. Geochemisty and petrogenesis of Urumiah-Dokhtar volcanics around Nain and Rafsanjan areas: a preliminary study. Treatise on the Geology of Iran, Iranian Ministry of Mines and Metals. 90 p.

Alavi M., 1994. Tectonic of the Zagros orogenic belt of Iran: new data and interpretations. Tectonophysics 229, 211-238.

Alavi M., 2007. Structures of the Zagros fold-thrust belt in Iran. American Journal of Science 307, 1064-95.

Allen M., Jackson J., Walker R., 2004. Late Cenozoic reorganization of the Arabia-Eurasia collision and the comparison of short-term and longterm deformation rates. Tectonics 23, TC2008, doi: 10.1029/2003TC001530.

Amidi S.M. and Emami M.H., 1984. Alkaline character of Eocene volcanism in the middle part of Central iran and its geodynamic situation. Geologische Rundschau 35, 917-932.

Anderson J.L., Smith D.R., 1995. The effect of temperature and fO_2 on the Al-in-hornblende barometer. American Mineralogist 80, 549-559.

Babaahmadi A., Safaei H., Yassaghi A., Vafa H., Naeimi A., Madanipour S., Ahmadi M., 2010. A study of Quaternary structures in the Qom region, West Central Iran. Journal of Geodynamics 50, 355-367.

Ballato P., Uba C.E., Landgraf A., Strecker M., Sudo M., Stockli D.F., Friedrich A., Tabatabaei S.H., 2011. Arabia-Eurasia continental collision: insights from late Tertiary foreland-basin evolution in the Alborz mountains, northern Iran. Geological Society of America Bulletin 123, 106-131.

Berberian F. and Berberian M., 1981. Tectono-plutonic episodes in Iran. In: Gupta H.K., Delany F., (Eds.), Zagros Hindukosh, Himalaya geodynamic evolution. American Geophysical Union, Washington DC., 5-32.

Berberian F., Muir F.I.D., Pankhurst R.J., Berberian M., 1982. Late cretaceous and early Miocene Andean type plutonic activity in northern Makran and central Iran. Journal of Geological Society 139, 605-614.

Berberian M. and King G.C.P., 1981. Towards a paleogeography and tectonic evolution of Iran. Canadian Journal of Earth Sciences 18, 210-265.

Bolourchi M.H., 1979. Explanatory text of the Kabudar Ahang quadrangle map, Iran, scale 1:250,000. Geological Survey of Iran.

Brown G.C., Thorpe R.S., Webb P.C., 1984. The geochemical characteristics of granitoids in contrasting arcs and comments on magma sources. Journal of Geological Society London 141, 413-426.

Cabanis B. and Lecolle M., 1989. Le diagramme La/10-Y/15-Nb/8: un outil pour la discrimination des séries volcaniques et la mise en évidence des processus de mélange et/ou de contamination crustale. Comptes Rendus de l'Académie des Sciences, Paris II 309, 2023-2029.

Condie K.C., 1989. Geochemical changes in basalts and andesites across the Archean-Proterozoic boundary: identification and significance. Lithos 23, 1-18.

Dargahi S., Arvin M., Pan Y., Babaei A., 2010. Petrogenesis of post-collisional A-type granitoids from Urumieh-Dokhtar magmatic assemblage, Southwestern Kerman, Iran: Constraints on the Arabian-Eurasian continental collision. Lithos 115, 190-204.

Deer W.A., Howie R.A., Zussman J., 1991. An Introduction to the Rock Forming Minerals (7^{th} impression). Longman Scientific Technical.

DePaolo D.J., 1981. Trace element and isotopic effects of combined wall rock assimilation and fractional crystallization. Earth and Planetary Science Letters 53, 189-202.

Dilek Y., Imamverdiyev N., Altunkaynak S., 2010. Geochemistry and tectonics of cenozoic volcanism in the lesser caucasus (Azerbaijan) and the peri-Arabian region: collision-induced mantle dynamics and its magmatic fingerprint. International Geology Review 52, 536-578.

D'Orazio M., Innocenti F., Manetti P., Haller M.J., 2004. Cenozoic back-arc magmatism of the southern extra-Andean Patagonia (44°30'-52°S): A review of geochemical data and geodynamic interpretations. Revista de la Asociación Geológica Argentina, 59, 525-538.

Elkins L.T. and Grove T.L., 1990. Ternary feldspar experiments and thermodynamic models. American Mineralogist 75, 544-559.

Emami M.H., 1991. Explanatory text of the Qom quadrangle map, Iran, scale 1:250,000. Geological Survey of Iran.

Ernst W.G. and Liu J., 1998. Experimental phase-equilibrium study of Al- and Ti-contents of calcic amphibole in MORB-A semiquantitative thermobarometer. American Mineralogist 83, 952-969.

Fan W.M., Gue F., Wang Y.J., Liu G., 2003. Late Mesozoic calcalkaline volcanism of post-orogenic extention in the northen Da Hinggan mountains, northeastern China. Journal of volcanology and geothermal research 121, 115-135.

Farhoudi G.H., 1978. A comparison of Zagros geology to island-arcs. Journal of Geology 86, 323-334.

Förster H., Feselfeldt K., Kursten M., 1972. Magmatic and orogenic evolution of the Central Iranial volcanic belt. 24^{th} Inter. Geology Congress, Montreal, Section 2, 198-210.

Gorton M.P. and Schandl E.S., 2000. From continents to island arcs: a geochemical index of tectonic setting for arc-related and within-plate felsic to intermediate volcanic rocks. Canadian Mineralogist 38, 1065-1073.

Helz R.T., 1973. Phase relations of basalts in their melting range at P_{H2O}=5 kb as a function of oxygen fugacity. Journal of Petrolology 17, 139-193.

Hessami K., Jamali F., Tabassi H., 2003. Map of Major Active Faults of Iran, Tech. rep., International Institute of Earthquake

Engineering and Seismology of Iran (IIEES), http://www.iiees.ir.

Holland T.B.J. and Blundy J.D., 1994. Non ideal in teractions in calcic- amphiboles and their bearning on amphibole-plagioclase thermometry. Contribution to Mineralogy and Petrology 11, 433-447.

Horton B.K., Hassanzadeh J., Stockli D.F., Axen G.J., Gillis R.J., Guest B., Amini A., Fakhari M.D., Zamanzadeh S.M., Grove M., 2008. Detrital zircon provenance of neoproterozoic to Cenozoic deposits in Iran: implications for chronostratigraphy and collisional tectonics. Tectonophysics 451, 97-122.

Huckriedre M., Kursten H., Venzlaff H., 1962. Zur geologie des gebiets zwischen Kerman und Saghand (Iran). Beihefte zum Geologischen Jahrbuch 51, 197 p.

Jazi M.A., Karimpour M.H., Malekzadeh A., 2012. A review on geochemistry and Rb/Sr and Sm/Nd isotopes of granitic intrusive bodies of middle Jurassic-Tertiary: a modern perspective on tectono-magmatism and mineralization in this period of Iran. Journal of Economic Geology (in Farsi with English Abstract) 4, 171-198.

Jung D., Kürsten M., Tarkian M., 1976. Post-Mesozoic volcanism inIran and its relation to the subduction of the Afro-Arabian under theEurasian plate. In: Pilger A., Rosler A., (Eds.), Afar between continental and oceanic rifting. Schweizerbartsche Verlag buchhandlung, Stuttgart. 175-181.

Kumar K.V., Rathna K., Leelanandam C., 2015 Proterozoic subduction-related and continental rift-zone mafic magmas from the Eastern Ghats Belt, SE India: geochemical characteristics and mantle sources. Current Science 108, 184-197.

Le Maitre R.W., Streckeisen A., Zanetti B., Le Bas M.J., Bonin B., Bateman P., Bellieni G., Dudek A., Efremova S., Keller J., Lameyre J., Sabine P.A., Schmid R., Sørensen H., Wooley A.R., 2002. Igneous rocks, a classification and glossary of terms. (Recommendations of the international union of geological sciences subcommission on the systematics of igneous rocks). Cambridge University Press, Cambridge, UK.

Leake B.E., Woolley A.R., Arps C.E.S., Birch W.D., Gilbert M.C., Grice J.D., Hawthorne F.C., Kato A., Mandarino J.A., Maresch W.V., Nikel E.H., Rock N.M.S., Schumacher J.C., Smith D.C., Stephenson N.C.N., Ungaretti L., Whittaker E.J.W., Youzhi G., 1997. Nomenclature of amphiboles: Report of the Subcommittee on Amphiboles of the International Mineralogical Association, Commission on New Minerals and Mineral Names. American Mineralogists 82, 1019-1037.

Leterrier J., Maury R.C., Thonon P., Girard D., Marchal M., 1982. Clinopyroxene composition as a methodof identification of the magmatic affinities of paleo-volcanic series. Earth and Planettary Science Letters 59, 139-154.

Lindsley D.H., 1983. Pyroxene thermometry. American Mineralogist 68, 477-493.

Mohajjel M., Fergusson C.L., 2000. Dextral trasnpression in Latecretaceous continental collision Sanandaj-Sirjan zone westernIran. Journal of Structural Geolology 22, 1125-1139.

Morimoto N., Fabrices J., Ferguson A.K., Ginzburg I.V., Ross M., Seifer F.A., Zussman J., Akoi K., Gottardi G., 1988. Nomenclature of pyroxenes. Mineralogical Magazine 52, 535-550.

Morley C.K., Kongwung P., Julapour A., Abdolghafourian M., Hajian M., Waples D., Warren J., Otterdoom H., Srisuriyon K., Kazemi H., 2009. Structural development of a major late Cenozoic basin and transpressional belt in central Iran: the central basin in the Qom-Saveh area. Geosphere 5, 1-38.

Nakamura N., 1974. Determination of REE, Ba, Fe, Mg, Na and K in carbonaceous and ordinary chondrites. Geochim Cosmochim Acta 35, 757-775.

Nisbet E.G., Pearce J.A., 1977. Clinopyroxene composition in mafic lavas from different tectonic settings. Contributions to Mineralogy and Petrology 63, 149-160.

Nogol-Sadate M.A.A., 1978. Les zones de decrochement et les virgations structurales en Iran. Concequences des resutants de I′analyse structural de la reigon de Qom: [Dissertation] Grenoble University, 201 p.

Nogol-Sadat M.A.A., 1985. Shear zones and structural bending in Iran, structural analysis results of Qom area. Report 55, Geological Survey of Iran.

Omrani J., Agard P., Whitechurch H., Benoit M., Prouteau G., Jolivet L., 2008. Arc magmatism and subduction history beneath the Zagros Mountains, Iran: a new report of adakites and geodynamic consequences. Lithos 106, 380-398.

Pearce J.A., 1983. Role of the sub-continental lithosphere in magma genesis at active continental margins. In: Hawkesworth C.J., Norry M.J., (Eds.), Continental Basalts and Mantle Xenoliths. Shiva, Nantwic. pp. 230-249.

Pearce J.A., 1982. Trace element characteristics of lavas from destructive plate boundaries. In: Thorpe R.S., (Eds.), Andesites. Wiley, Chichester. 525-548.

Polliand M., Schaltegger U., Frank M., Fontboté L., 2005. Formation of intra-arc volcanosedimentary basins in the western flank of the central Peruvian Andes during Late Cretaceous oblique subduction: field evidence and constraints from U-Pb ages and Hf isotopes.International Journal of Earth Sciences/Geologische Rundschau 94, 231-242.

Putirka K.D., 2008. Thermometers and Barometers for Volcanic Systems. Reviews in Mineralogical Society of America 69, 61-120.

Rezaeian, M., Carter, A., Hovius, N., Allen, M.B. 2012. Cenozoic exhumation history of the Alborz Mountains, Iran: New constraints from low-temperature chronometry. Tectonics, 31, TC2004, doi: 10.1029/2011TC002974.

Ridolfi F., Renzulli A., Puerini M., 2010. Stability and chemical equilibrium of amphibole in calk-alkaline magmas: an overview new thermobarometric formulations and applications to subduction-related volcanoes. Contributions to Mineralogy and Petrology 160, 45-66.

Rollinson H.R., 1993. Using Geochemical data: Evaluation, presentation, Interpretation. Longman group UK Ltd. London, United Kingdom.

Rudnick R.L. and Gao, S., 2003. The composition of the continental crust. In: Rudnick, R.L., (Eds.), The Crust. Elsevier-Pergamon, Oxford, 1-64.

Schmidt M.W., 1992. Amphibole composition in tonalite as a function of pressure: An experimental calibration of the AI-in-hornblende barometer. Contributions to Mineralogy and Petrology 110, 304-310.

Schröder J.W., 1944. Essai sur la structure de l'Iran. Eclogae Geologicae Helvetiae 37, 37-81.

Spear F.S., 1981. An experimental study of hornblende stability and compositional variability inamphibolites. American Journal of Science 281, 697-734.

Stöcklin J., 1974. Possible ancient continental margins in Iran. In: Burk C.A., Drake C.L., (Eds.), The Geology of Continental Margins. Springer-Verlag, Berlin 873-887.

Sun S.S. and McDonough W.F., 1989. Chemical and isotopic systematic of oceanic basalts: implications for mantle composition and processes. Magmatism in the ocean basins: In: Saunders A.D., Norry M.J. (Eds.), Geological Society, London, Special Publications 42, 313-345.

Tabatabaeimanesh S.M., Safaei H., Mirlohi A.S., 2011. Geotectonic investigation of early Paleozoic magmatism in Urumieh-Dokhtar zone (south of Kashan). Geosciences (in Farsi with English Abstract) 20, 47-52.

Tatsumi Y., Nakashima T., Tamura Y., 2002. The petrology and geochemistry of calc-alkaline Andesite on shodo-Shima Island, SW Japan. Journal of Petrology 43, 3-16.

Taylor S.R., McLennan S.M., 1985. The continental crust: its composition and evolution. Blackwell, Oxford.

Taylor S.R., McLennan S.M., 1995. The geochemical evolution of the continental crust. Reviews of Geophysics 33, 241-265.

Varekamp J.C., Hesse A., Mandeville C.W., 2010. Back-arc basalts from the Loncopue graben (Province of Neuquen, Argentina). Journal of Volcanology and Geothermal Research 197, 313-328.

Verdel C., Wernicke B.P., Hassanzadeh J., Guest B., 2011. A Paleogene extensional arc flare-up in Iran. Tectonics 30, TC3008, doi:10.1029/2010TC002809.

Vincent S.J., Allen M.B., Ismail-Zadeh A.D., Flecker R., Foland K.A., Simmons M.D., 2005. Insights from the Talysh of Azerbaijan into the Paleogene evolution of the South Caspian region. GSA Bulletin 117, 1513-1533.

Vincent S.J., Morton A.C., Carter A., Gibbs S., Barabadze T.G., 2007. Oligocene uplift of the Western Greater Caucasus: An effect of initial Arabia-Eurasia collision. Terra Nova 19, 160-166.

Walker R.T. and Jackson J., 2004. Active tectonics and late Cenozoic strain distribution in central and eastern Iran. Tectonics 23, doi: 10.1029/2003TC001529.

Wood D.A., 1980. The application of a Th-Hf-Ta diagram to problem of tectonomagmatic classification and to establishing the nature of crustal contamination of basaltic lavas of the British tertiary volcanic province. Earth Planetary Science Letters 50, 11-30.